On the use of fractal surfaces to understand seismic wave propagation in layered basalt sequences

Catherine E. Nelson[1], Richard W. Hobbs[2] and Roxanne Rusch[2]

[1]Previously at Department of Earth Sciences, Durham University, Durham DH1 3LE

[2]Department of Earth Sciences, Durham University, Durham DH1 3LE

Abstract

The aim of this study is to better understand how a layered basalt sequence affects the propagation of a seismic wave, which has implications for sub-basalt seismic imaging. This is achieved by the construction of detailed, realistic models of basalt sequences, using data derived directly from outcrop analogues. Field data on the surface roughness of basaltic lava flows was captured using terrestrial laser scanning and satellite remote sensing. The fractal properties of the surface roughness were derived, and it can be shown that the lava flow surface is fractal over length scales up to approximately 2km. The fractal properties were then used to construct synthetic lava flow surfaces using a von Karman power spectrum, and the resulting surfaces were then stacked to create a synthetic lava flow sequence. P-wave velocity data were then added and the resulting model was used to generate synthetic seismic data. The resulting stacked section shows that the ability to resolve the internal structure of the lava flows is quickly lost due to scattering and attenuation by the basalt pile. A further result from generating wide angle data is that the appearance of a lower velocity layer below the basalt sequence may be caused by destructive interference within the basalt itself.

Introduction

Reliable sub-basalt seismic imaging remains an outstanding problem in exploration geophysics. Several strategies have been developed to improve seismic imaging beneath basalt sequences, such as deep towed streamers to boost the low frequency content (e.g. Davison et al., 2010). However, scattering and attenuation of the seismic energy by the basalt sequence means that very little energy reaches a sub-basalt sedimentary succession. The greatest challenges to sub-basalt seismic imaging are caused by continental flood basalt provinces, where basalt thicknesses can range from hundreds of metres to several kilometres.

One motivating factor for research into seismic imaging below flood basalt provinces is the possible presence of hydrocarbon-bearing basins beneath. In the North Atlantic, sedimentary basins with known hydrocarbon discoveries extend below the edge of the basalt sequences of the North Atlantic Igneous Province. Additionally, one significant discovery has been made within the area covered by the basalt (Helland-Hansen, 2009), and oil has been observed within the basalt itself (Laier et al., 1997). The Kutch Basin, onshore and offshore northwest India, is another area thought to have substantial sub-basalt prospectivity (Kumar et al., 2004; Rohrman, 2007).

A continental flood basalt province (CFBP) consists of an abnormally voluminous sequence of volcanic material, often thought to be formed from mantle plume material (e.g. Saunders, 2005). Examples include the Paleogene North Atlantic Igneous Province, the Cretaceous-Tertiary Deccan Traps, and the Permian-Triassic Siberian Traps. Generally, lava flows are the most common eruptive product, though there can also be substantial volumes of hyaloclastites and pyroclastic material (White et al., 2009).

The lava flows in a CFBP are most commonly of pahoehoe type (Self et al., 1998), and can be tens of metres thick, extending laterally for tens of kilometres continuously, or can be

just a few metres thick or less, with an anastomosing, braided architecture (Jerram, 2002). Volumes of individual lava flows can be over 1,000 km^3 dense rock equivalent (Bryan et al., 2010). Each lava flow has a three-part vertical division with a rubbly, vesicular top; a massive, relatively unfractured core; and a vesicular base. This three-part division means that the rock properties of each lava flow are highly heterogeneous: the crust and base have a low P-wave velocity and density, and the core has a much higher velocity and density (Planke, 1994). A stack of lava flows therefore exhibits strong layering of its acoustic impedance. It has been shown that the attenuation of a seismic wave caused by a thick basalt sequence is due to a combination of both this layering, and scattering caused by the rough surface of the lava flows (Maresh et al., 2006, discussed further in Nelson et al., 2009a). High frequencies are preferentially attenuated, so the returned energy is predominantly at a low frequency.

In this study, we seek to better understand the effect of a layered basalt sequence on seismic wave propagation, so that the results can be used to improve sub-basalt seismic imaging. This is achieved by the use of models that accurately capture the heterogeneity within a layered basalt sequence. These must have a vertical resolution of tens of centimetres to accurately model this heterogeneity (Martini et al., 2005). Ideally, these would be deterministic models constructed from data collected from flood basalt outcrops. However, there are several features of flood basalt provinces in the field that make this difficult:

- **Incomplete exposure:** To map the extent of a lava flow, it is necessary to know the position of all the edges of the flow. This is easy for recent, uneroded lava flows, but extremely difficult when a lava flow is buried by many subsequent flows.

- **Poor exposure.** Basalt weathers easily and is often covered by vegetation or scree.

- **Difficulty in correlation.** Lava flows within a flood basalt province can be of a similar composition, and have a similar physical appearance. If no marker horizons (such as

sedimentary layers) are present it can be extremely difficult to correlate flows between outcrops - especially as they may change in thickness between two outcrops.

Accordingly, in this work we derive the fractal properties of field exposures of basaltic lava flows, and use these to construct synthetic lava flow surfaces. The incorporation of the field data makes the models more realistic, and the surfaces can be generated at any scale required.

Background and previous work

Many geological and topographic features are scale-invariant, meaning they can be described by a fractal dimension, D (Turcotte, 1989). It is possible to test whether a medium is fractal by taking the Fourier transform of a profile across it to generate a power spectrum. A fractal medium displays a relationship between the power spectrum and wave number given by the following equation (Huang and Turcotte, 1989):

$P(k)=Ak^{\beta}$

where $P(k)$ is the power spectrum, k is the wavenumber and A is a constant. If the power spectral density is plotted against the wavenumber on a log-log scale (Figure 1), β is given by the slope of the straight line part. The fractal dimension D can be calculated from the

slope as follows (Higuchi, 1990):
$$D = \frac{2E+3-\beta}{2}$$

where E is the Euclidean dimension. For a one dimensional profile, $E = 1$, for a two dimensional surface $E = 2$, and so on.

For the one-dimensional case (i.e. a cross-section of a surface), the equation is therefore as follows: (Huang and Turcotte, 1989; Dolan and Bean, 1997).

$$D = \frac{5 - \beta}{2}$$

The upper limit of the straight line in Figure 1 is the correlation length a, and beyond this the medium is no longer fractal (Frenje, 2000). If a 1D profile across a basalt lava flow surface shows this type of plot we know it is fractal at scales up to the correlation length.

Figure 1 Determining Hurst number and correlation length from a power spectrum.

The Hurst number is also used to quantify the fractal properties of a medium, and is useful for comparison between 1D and 2D fractal parameters. The Hurst number, H (or ν) is related to D by the following equation (Mandelbrot, 1985; Feder, 1988; Dolan and Bean, 1997):

$$D = E + 1 - H$$

The effect on surface roughness of altering the Hurst number is shown in Figure 2.

Figure 2: Effect of the Hurst number on surface roughness, while the standard deviation remains constant. From Saupe (1988).

Previous studies have considered the tops of basalt lava flow successions as fractal surfaces. Walia and Bull (1997) analysed seismic data from the Rockall Trough, using spectral analysis to obtain a fractal dimension of 1.36, corresponding to a Hurst number of 0.7 for the top surface of the lava pile. Martini et al. (2005) used this value to construct 3D velocity models, along with a fractal dimension for the vertical velocity distribution obtained from a large dataset of Ocean Drilling Program wells. Maresh (2004) analysed 3D seismic data from the Rockall Trough, obtaining a 2D fractal dimension of 2.49, equating to a Hurst number of 0.51. However, these results cannot be taken as representative of individual flows: because of the resolution limit (quarter wavelength) of band-limited seismic data it is impossible to know whether the top surface of the basalt sequence is one flow or many.

Bean and Martini (2010) used digital photographs of a single lava flow from the Tertiary Basalt Province of Northern Ireland to obtain a Hurst number of 0.2. This is substantially different to the results of Walia and Bull (1997) and of Maresh (2004). This difference is likely to be because the surface chosen by Bean and Martini (2010) is the interface between the base of the basalt succession and the top of a limestone sequence. The roughness of this surface is controlled by the erosion of the limestone, which is then passively infilled by

the lava flow, making this result useful for modelling the base of a basalt succession. It does not represent the roughness of an individual lava flow.

Much of this work stems from analysis of borehole data to produce stochastic models (e.g. Bean, 1996; Holliger, 1996; Dolan and Bean, 1997; Dolan et al., 1998; Frenje and Juhlin, 1998) and analysis of topography both on land (Huang and Turcotte, 1989) and on the seafloor (Goff and Jordan, 1988). Similar approaches have been used in a number of different fields including the analysis of sedimentary cycles (Browaeys and Fomel, 2009) and in seismic oceanography (Buffett et al., 2010).

Fractal surfaces are also observed in other geological settings, for example stylolites (e.g. Ebner et al., 2009; 2010). Laronne Ben-Itzhak et al. (2012) used terrestrial laser scanning of stylolite surfaces up to 10m long to derive their Hurst numbers and correlation length. The roughness of fault surfaces has also been shown to be fractal, at length scales from millimetres to thousands of kilometres (Renard et al., 2013).

Field data for fractal analysis

For this study, three datasets were available for fractal analysis. The datasets are known to be from single lava flows, at scales covering 10cm to 10km. Two datasets are from modern lava flows, where the top lava flow surface has not been subject to significant weathering, and the third is from part of the Paleogene North Atlantic Igneous Province.

Glyvursnes

The first dataset comes from a quarried exposure near Glyvursnes, on the island of Streymoy, Faroe Islands. This outcrop, shown in Figure 3 below, was chosen because it offered a very clear top surface of one lava flow and a base surface of another, with a sedimentary bole horizon in the middle. The top and base are very well-preserved and offer an excellent 2D section for analysing the surface roughness. It is within the Enni Formation of the Faroe Islands Basalt Group, part of the NAIP.

Surface roughness data in this location were acquired using terrestrial laser scanning, allowing the outcrop geometry to be accurately captured in digital format. This equipment has become increasingly popular amongst geologists, as it allows 3D data to be captured which can be analysed away from a field situation. 3D point clouds thus obtained can be analysed to provide quantitative structural or geological data (e.g. McCaffrey et al. 2005, 2008; Nelson et al., 2011). The laser scanner measures the XYZ coordinates of points on the outcrop at specified intervals by calculating the distance from the scanner based on the return time of the laser beam. These points can then be coloured from digital photos to give an accurate representation of the outcrop, which can then be viewed from any angle and features on it can be measured. This is particularly useful for inaccessible parts of outcrops. Multiple scans from different angles are obtained to minimise shadow areas where parts of the outcrop hide other areas from

the scanner viewpoint. Reflectors are used to provide common points of reference between scan and photo, and between scans. Previous studies have documented in detail the standard workflow for capturing and processing TLS data (e.g. Buckley et al., 2007; Enge et al., 2007).

The equipment used in this work is a Riegl LMS-Z420i terrestrial laser scanner (Figure 3 (a)), frequently used in geology and optimized for rapid data acquisition, a long range and usage in demanding environmental conditions. Two scans were required for complete coverage of this outcrop because its geometry was relatively simple. A total of approximately 8,200,000 points were collected, and 14 digital photographs in two panoramic sequences. The flow top and base were identified on the digital photographs, and 3D lines were drawn on the scan surface following the methods described in Nelson et al. (2011), shown in Figure 3 (d). The total length of the outcrop is approximately 130m. Approximately 700 points were digitized for the base of the upper flow, giving an average point spacing of around 17cm. Approximately 900 points were digitized for the top of the lower flow, giving an average point spacing of around 15cm. These were converted to 2D profiles along the top and base of the flows, suitable for the generation of power spectra.

Figure 3: Laser scan data from coastal quarry at Glyvursnes. Outcrop height is approximately 10m. a) Acquiring the laser scan data. b) The quarry wall with photo-interpretation of the lava flow top and base. c) The completed scan data. d) Lines interpreted from the scan data.

Erta Ale

The second dataset available for this work comprised terrestrial laser scanning data from Erta Ale volcano, Ethiopia. This is a remote and rarely visited active basaltic volcano, with a lava lake and surrounding crater. The lava lake is one of the oldest known, having persisted for over 90 years (Oppenheimer and Francis, 1998). Data used here are taken from the crater floor surrounding the lava lake. The crater floor is covered by pahoehoe lava flows

formed when the lava lake overflows (Field et al., 2012). This provides a large fresh surface with the opportunity of taking many profiles in any direction. The area of interest is approximately 80 by 125m.

Data were collected by Dougal Jerram and Steve Smith as part of filming for the BBC1 television series "The Hottest Place on Earth" (Jerram and Smith, 2010). A total of 6 scans were required to completely capture the crater, and approximately 24,000,000 points and 42 digital photographs were collected. The coloured 3D point cloud is shown in Figure 4. 2D profiles were captured directly from the scan data, and the resulting sections have a length of 70-125m and a point spacing of approximately 10cm. Two sections were chosen for further analysis: the longest possible sections in orthogonal directions, along and across the crater floor.

Figure 4: Laser scan data from Erta Ale, Ethiopia. Photographs courtesy of Dougal Jerram. a) Collecting the scan data. b) Overview of the crater and surroundings. c) Complete scan data and scan positions.

Laki

The third dataset is a satellite digital elevation model (DEM) covering the Laki lava flow, Iceland. This was emplaced in 1783-84 and is regarded as the closest modern analogue to a flood basalt lava flow (Self et al., 1998). It has been used to model the environmental impact of flood basalt eruptions (Self et al., 2006) and has also been used as an analogue to Martian lavas (Keszthelyi et al., 2004). Thordarson and Self (1993) and Guilbaud et al. (2005) provide a full description of the flow morphology and its eruption. Cross-sections through the Laki lava flow and the Roza Member of the Columbia River flood basalt province reveal the same three-part internal structure (Self et al., 1998).

The Laki lava field totals approximately 14.7km^3 of basaltic lava, covering an area of approximately 599km^2 (Thordarson and Self, 1993). The lava erupted from fissures in the Sída highlands of southern Iceland, part of the Grimsvotn volcanic system, and flowed south down the gorges of two rivers: the Skaftá and the Hverfisfljót. It then spread out onto the flat coastal plain formed by the earlier Eldgja lava flow (934AD). The area of interest for this study, shown in Figure 5, is the branch that flowed out of the Skaftá gorge onto the coastal plain - the Eldhraun branch. This comprises ~5km^3 of lava that was emplaced directly onto the Eldgja lava, into an unconfined area. This area is therefore a useful analogue for a flood basalt lava flow.

Figure 5: Eldhraun branch of the Laki lava flow: location map and satellite DEM from ASTER Global Digital Elevation Model (http://www.gdem.aster.ersdac.or.jp/). Data at 30m resolution. Original data of ASTER GDEM is the property of the Ministry of Economy, Trade and Industry (Japan) and NASA. Flow directions and Laki extent from Guilbaud et al. (2005).

The Eldhraun branch is also useful because it offers a very large distance to analyse – approximately 15km profiles can be made as shown in Figure 5. As it is so young, and remains uncovered by any later lava flows, it preserves its surface morphology very well, as shown in Figure 6. Two cross-sections were taken from this dataset, one across the flow direction and one along the flow direction, as shown in Figure 5. The along-flow section has a length of 23.7km, with a point spacing of approximately 23m, and the across-flow section has a length of 15.1km, with a point spacing of approximately 15m.

Figure 6: Laki surface roughness. a) Eldhraun branch near Kirkjubaejarklaustur. b) Looking south across the Eldhraun from Fjaðrárgljúfur.

Spectral analysis

1D profiles were taken through each of the datasets described above, and power spectra were calculated for each profile. The Generic Mapping Tools (GMT) software was used to analyse the data (Wessel and Smith, 2009). This is an open source set of tools for manipulating x,y and x,y,z data, available to download from http://gmt.soest.hawaii.edu/. Spectral density estimates follow the method of Welch (1967) and error bars are produced following the method of Bendat and Piersol (1986).

The resulting power spectra are shown in Figure 7 below. There is a good agreement between datasets at each location. The Laki power spectra (Figure 7a) show a very close agreement between the section along and across the flow, suggesting that the roughness is approximately isotropic and the same fractal properties can be used in both directions. This spectrum also displays a clear roll-over point, indicating that the surface can be treated as fractal up to around 2000m (the correlation length).

The data from Glyvursnes show that there is no significant difference between the roughness of a flow top and flow base. For values below approximately 20cm (2 on the x axis in Figure 7b) the wavelength is equal to the spacing of the data points, so the results are not useful. The same applies to the results from Erta Ale. Again, there is no significant anisotropy apparent in the surface roughness.

Figure 7: Power spectra of data from a) Laki, b) Glyvursnes and c) Erta Ale.

The data from Laki, Glyvursnes and Erta Ale are plotted together in Figure 8. A best fit line can be drawn within the uncertainties of the data. From this, a β value (slope) of 2.1 is measured (derived from a 1D Fourier transform). Using the equations described earlier, a Hurst number of 0.55 is obtained. As discussed above, the correlation length is 2000m.

The dashed lines in Figure 8 give an estimate of the error on the Hurst number: the likely range is around 0.5-0.65. It can be seen that there is a slight step between the data from Laki and the laser scan data, and this is likely to be due to the change in instrumentation. However, this is within the errors of the data, so a simple single slope was chosen to describe the surface, consistent with the individual slopes from each dataset and previous work. Data at scales in between the satellite data and the laser scan data would help to verify this.

Model construction

The Hurst number of 0.55 and correlation length of 2000m derived in the previous section were used to build synthetic surfaces with the same statistical properties as the real surfaces. The random volume building code developed by White (2009) for building velocity models of basalt sequences was adapted to produce surface topography. The code generates either 2D surfaces or 3D fractal volumes using a von Karman power spectrum with specified correlation lengths, standard deviations in the two or three Cartesian coordinates, as required, and a Hurst number. Here we use the code to generate surfaces that represent lava flow top surfaces, using the fractal properties derived in the previous section. Figure 9 shows a final surface composed of 512 nodes in both the x and y directions, with a horizontal grid node spacing of 20m, giving an overall size of 10.22 x 10.22km.

Figure 9: Fractal model produced with the random volume building code of White (2009).

The surfaces can then be stacked to simulate flows of various thicknesses and types. First, the types of volcanic facies required in the model is given along with the mean flow thickness and standard deviation, as determined from mapping in the field, and the number of flows in the basalt pile. The facies types can be any of the following:

- Tabular lava flows, which tend to be the thicker layers, include a massive core with a crust and base (Planke, 1994)

- Compound lava flows without a massive core (Jerram, 2002)

- Volcaniclastics, with a uniform structure (representing hyaloclastites or pyroclastic deposits). Hyaloclastites have been shown to have a narrow, relatively uniform velocity distribution (Nelson et al., 2009b).

- Sedimentary sequences with a uniform structure.

The process is iterative starting with the lowermost layer. The base of the basalt pile may be horizontal representing an erosional surface, or with topography if that can be predicted from field mapping. A fractal surface is generated that represents the top of the first flow, a thickness is drawn from the specified population using a random number generator and a facies type is selected from a weighted probabilistic list such that over a significant number of flows (> 10) the number of each facies type approaches the expected probability. The interior structure of the flow is constructed depending on the facies type. Again, this internal structure is preconditioned on a set of probabilistic functions determined from the field which, as in the case of geophysical models demonstrated here, will include data from well logs (e.g. Nelson 2010). The process of generating layer top, thickness and facies type is repeated until the required number of layers is reached. At this point the whole cycle can be repeated but with a new set of probabilistic functions for thickness, flow-type, internal structure to represent the different phases in the evolution of a flood-basalt province. The final model can be arbitrarily complex, as the probabilistic descriptors and fractal surfaces can be applied to any length-scale. A cross-section through a possible model is shown in Figure 10.

Figure 10: 2D section through a 3D probabilistic model for a sequence of flows that have built up a 2km thick basalt-dominated pile, which has then subsided and been buried by later sediments (similar to the Faroe-Shetland trough). The model is coloured by seismic P-wave velocity, but it could equally be coloured by density, S-wave velocity, or geological descriptors.

The geophysical model shown in Figure 10 is then used to help understand seismic wave propagation. Two possible outputs are shown in Figure 11. By using viscoelastic complex-screen modelling (White and Hobbs, 2007), it is possible to generate an ideal stacked section. The high-impedance contrasts at the top of the basalt pile form the brightest reflections. The ability to resolve the internal structure is quickly lost as scattering by the rough surfaces

and internal reverberation absorbs the higher frequencies and destroys the coherency of the wavefront, which is consistent with the result seen by Maresh et al. (2006).

The second and possibly more interesting result is the wide-angle response computed using finite difference code (Cohen and Stockwell, 2012). The first arrival from the basalt shows a characteristic response of an event that appears to be truncated with a step-back in time to the event associated with the deeper basement. This characteristic is widely interpreted as evidence of lower velocity sediments beneath the basalt layer (e.g. Raum et al., 2005). This interpretation is based on the high frequency ray-tracing approximation with a homogeneous basalt layer with a velocity gradient where the truncation of the basalt refraction corresponds to the grazing ray that just stays within the basalt layer. However, as demonstrated by this model, it is possible to generate the same effect in a model with no internal gradient, but solely by destructive interference of scattered energy.

Figure 11: (a) Ideal primary only seismic reflection section from the model in figure 10 showing the rapid loss of back-scattered energy from the basalt sequence. In reality, the received image will be significantly degraded by the inclusion of the multiply scattered energy that will appear as noise on the section. (b) The corresponding long-offset refraction model. Note the termination of the basalt refraction event caused by multiple destructive interference of scattered energy which is dominated by scattering in the upper layers of the model.

Discussion

This study has shown that spectral analysis is a valid method for understanding the properties of a basalt lava flow surface, and that the surface can be considered as fractal up to the correlation length of 2000m. Having obtained the correlation length and Hurst number (0.55) it is possible to construct random surfaces with the same statistical properties as the real surfaces.

The result of 0.55 for the Hurst number achieved here is similar to that of Walia and Bull (1997), and also in good agreement with Maresh (2004), as discussed earlier. It is substantially different from that of Bean and Martini, but again as discussed earlier this is likely because their result is taken from the base of a flow overlying eroded limestone. The datasets presented here are known to be from fresh, unaltered top surfaces of lava flows. The result of Bean and Martini would be of use in modelling the base surface of a flood basalt province; however the data presented here are useful for modelling internal reflectors and the top surface.

Another issue for discussion is the correlation length. Here, I use the same value of 2000m for both along flow and across flow directions. White (2009) used a correlation length ten times larger in one direction than the other, citing Thomson (2005). Martini et al. (2005), working along similar lines, used a correlation length five times greater in one horizontal direction than the other. This is appropriate for lava flows emplaced onto dipping surfaces, however Thomson (2005) also described flat-lying flows of roughly equant x-y dimensions, similar to our results from Laki. The dip of the required flows should be taken into account when developing a model of a flood basalt province, as lava flows emplaced onto a dipping surface will display longer correlation lengths along the direction of flow. The correlation length can easily be altered in the random volume code of White (2009) to reflect the desired geometry.

The methods presented here for constructing random surfaces are useful in situations where the entire scale length of a feature cannot easily be captured. It is relatively easy to characterize the surface of a lava flow at the outcrop scale (10s of metres) and satellite data allows features to be measured at 100s of metres to kilometre scales; however in between this it becomes more difficult. Satellite data is not easily obtained at a resolution of below 30-50m, and outcrops larger than 100-200m are rare and difficult to measure. The use of fractal modelling covers this scale gap. One problem with studying flood basalt provinces is that exposure is often incomplete, and it is impossible to tell the extent of a single lava flow as the edges are not preserved or are difficult to correlate. By bringing together these diverse datasets it is possible to build realistic models of lava flow surfaces without the need for correlation between outcrops or time-consuming mapping.

Having determined the statistics of the basalt surface and probabilistic descriptors of the internal structure of the various basalt facies, it is then possible to construct constrained models that can be used to investigate the combined effects of rough surfaces and complex high-impedance internal structure on seismic wave propagation. Below the top of the basalt surface, the reflections quickly die off in amplitude and do not correspond to the layering in the model. An interesting result is that an apparent velocity step-back below the basalt sequence can be created in wide angle data by scattering within the basalt. This could lead to the interpretation of a sedimentary basin below the basalt sequence where none in fact exists. Further work should explore different geological scenarios using these models, varying the thickness of both the basalt layer and the sedimentary basin, to understand what interpretations are possible.

Acknowledgements

References

Bean, C.J. (1996), On the cause of 1/f-power spectral scaling in borehole sonic logs, Geophysical Research Letters 23, 3119-3122.

Bean, C.J., and Martini, F. (2010), Sub-basalt seismic imaging using optical-to-acoustic model building and wave equation datuming processing, Marine and Petroleum Geology 27, 555-562.

Bendat, J.S., and Piersol, A.G., Random data: Analysis and measurement procedures, (John Wiley, New York 1986)

Browaeys, T.J., and Fomel, S. (2009), Fractal heterogeneities in sonic logs and low-frequency scattering attenuation: Geophysics 74, WA77-WA92.

Bryan, S. E., Peate, I.U., Peate, D.W., Self, S., Jerram, D.A., Mawby, M.R., Marsh, J.S., and Miller, J.A. (2010), The largest volcanic eruptions on Earth, Earth-Science Reviews 102, 207-229.

Buckley, S.J., Howell, J.A., Enge, H.D., and Kurz, T.H. (2008), Terrestrial laser scanning in geology: data acquisition, processing and accuracy considerations, Journal of the Geological Society 165, 625-638.

Buffett, G.G., Hurich, C.A., Vsemirnova, E.A., Hobbs, R.W., Sallares, V., Carbonell, R., Klaeschen, D., and Biescas, B. (2010), Stochastic heterogeneity mapping around a Mediterranean salt lens, Ocean Science 6, 423-429.

Cohen, J. K. and Stockwell, Jr. J. W., (2012), CWP/SU: Seismic Un*x Release No.43r3: an open source software package for seismic research and processing, Center for Wave Phenomena, Colorado School of Mines.

Davison, I., Stasiuk, S., Nuttall, P., Keane, P. (2010), Sub-basalt hydrocarbon prospectivity in the Rockall, Faroe-Shetland and Møre basins, NE Atlantic, in B. A. Vining, S. C. Pickering, ed., Petroleum Geology: From Mature Basins to New Frontiers - Proceedings of the 7th Conference, The Geological Society of London, 1025-1032.

Dolan, S.S., and Bean, C.J. (1997), Some remarks on the estimation of fractal scaling parameters from borehole wire-line logs, Geophysical Research Letters 24, 1271-1274.

Dolan, S.S., Bean, C.J., and Riollet, B. (1998), The broad-band fractal nature of heterogeneity in the upper crust from petrophysical logs, Geophysical Journal International 132, 489-507.

Ebner, M., D. Koehn, R. Toussaint and F. Renard, (2009) The influence of rock heterogeneity on the scaling properties of simulated and natural stylolites, J. Struct. Geol., 31, 72

Ebner, M., R. Toussaint, J. Schmittbuhl, D. Koehn and P. Bons, (2010) Anisotropic scaling of tectonic stylolites: a fossilized signature of the stress field? , J. Geophys. Res., 115, B06403.

Enge, H.D., Buckley, S.J., Rotevatn, A., and Howell, J.A. (2007), From outcrop to reservoir simulation model: Workflow and procedures, Geosphere 3, 469-490.

Feder, J. Fractals (Plenum Press, New York, 1988).

Field, L., Barnie, T., Bludy, J., Brooker, R.A., Keir, D., Lewi, E. and Saunders, K. (2012), Integrated field, satellite and petrological observations of the November 2010 eruption of Erta Ale, Bulletin of Volcanology 74, 2251-2271.

Frenje, L., Scattering of Seismic Waves in Random Velocity Models (PhD thesis, Uppsala University 2000).

Frenje, L. and Juhlin, C. (1998), Scattering of seismic waves simulated by finite difference modelling in random media: application to the Gravberg-1 well, Sweden, Tectonophysics 293, 61-68.

Guilbaud, M., Self, S., Thordarson, T., and Blake, S. (2005), Morphology, surface structures, and emplacement of lavas produced by Laki, AD 1783-1784, Special paper- Geological Society of America 396, 81-102.

Helland-Hansen, D. (2009), Rosebank - Challenges to development from a subsurface perspective, in Varming, T., and Ziska, H., eds., Faroe Islands Exploration Conference: Proceedings of the 2nd Conference, Annales Societatis Scientarium Faroensis, supplementum 50, 241-245.

Higuchi, T. (1990). "Relationship between the fractal dimension and the power law index for a time series : A numerical investigation", Physica D 46, 254-264.

Holliger, K. (1996), Upper-crustal seismic velocity heterogeneity as derived from a variety of P-wave sonic logs: Geophysical Journal International 125, 813-829.

Huang, J., and Turcotte, D.L. (1989), Fractal Mapping of Digitized Images: Application to the Topography of Arizona and Comparisons With Synthetic Images: Journal of Geophysical Research 94, 7491-7495.

Jerram, D.A. (2002), Volcanology and facies architecture of flood basalts, in Menzies, M.A., Klemperer, S.L., Ebinger, C.J., and Baker, J., eds., Volcanic rifted margins. Geological Society of America Special Paper 362, 119-132.

Jerram, D.A., and Smith, S.A.F. (2010), Earth's hottest place, Geoscientist 20, 12-13.

Keszthelyi, L., Thordarson, T., McEwen, A., Haack, H., Guilbaud, M.N., Self, S., and Rossi, M.J. (2004), Icelandic analogs to Martian flood lavas, Geochemistry Geophysics Geosystems 5, 1-32.

Kumar, D., Bastia, R., and Guha, D. (2004), Prospect hunting below Deccan basalt: imaging challenges and solutions: First Break 22, 35-39.

Laier, T., Nycroft, H.P., Jørgensen, O., and Isaksen, G.H. (1997), Hydrocarbon traces in the Tertiary basalts of the Faeroe Islands, Marine and Petroleum Geology 14, 257-266.

Laronne Ben-Itzhak, L., E. Aharonov, R. Toussaint and A. Sagy, (2012) Upper bound on stylolite roughness as indicator for the duration and amount of dissolution, Earth and Planetary Science Letters, 337-338, 186-196

McCaffrey, K.J.W., Feely, M., Hennessy, R., and Thompson, J. (2008), Visualization of folding in marble outcrops, Connemara, western Ireland: An application of virtual outcrop technology, Geosphere 4, 588-599.

McCaffrey, K.J.W., Jones, R.R., Holdsworth, R.E., Wilson, R.W., Clegg, P., Imber, J., Holliman, N., and Trinks, I. (2005), Unlocking the spatial dimension: digital technologies and the future of geoscience fieldwork,: Journal of the Geological Society 162, 927-938.

Mandelbrot, B. (1985), Self-Affine Fractals and Fractal Dimension. Physica Scripta 32, 257-260.

Maresh, J. The Seismic Expression of Paleogene Basalts on the Atlantic Margin (PhD thesis, Cambridge University, 2004).

Maresh, J., White, R.S., Hobbs, R.W., and Smallwood, J.R. (2006), Seismic attenuation of Atlantic margin basalts: Observations and modeling, Geophysics 71, B211-B221.

Martini, F., and Bean, C.J. (2002), Application of pre-stack wave equation datuming to remove interface scattering in sub-basalt imaging, First Break 20, 395-403.

Martini, F., Hobbs, R.W., Bean, C.J., and Single, R. (2005), A complex 3-D volume for subbasalt imaging, First Break 23, 41–51.

Nelson, C.E., Jerram, D.A., Hobbs, R.W., Terrington, R., and Kessler, H. (2011). Reconstructing flood basalt lava flows in 3D using terrestrial laser scanning, Geosphere 7, 87-96.

Nelson, C.E., Methods for constructing 3D geological and geophysical models of flood basalt provinces, (PhD thesis, Durham University 2010).

Nelson, C.E., Jerram, D.A., Single, R.T., and Hobbs, R.W. (2009a), Understanding the facies architecture of flood basalts and volcanic rifted margins and its effect on geophysical properties., in Varming, T., and Ziska, H., eds., Faroe Islands Exploration Conference: Proceedings of the 2nd Conference, 84-103.

Nelson, C.E., Jerram, D.A., and Hobbs, R.W. (2009b), Flood basalt facies from borehole data: implications for prospectivity and volcanology in volcanic rifted margins, Petroleum Geoscience 15, 313-324.

Oppenheimer, C., and Francis, P. (1998), Implications of longeval lava lakes for geomorphological and plutonic processes at Erta Ale volcano, Afar, Journal of Volcanology and Geothermal Research 80, 101-111.

Planke, S. (1994), Geophysical response of flood basalts from analysis of wire line logs: Ocean Drilling Program Site 642, Vøring Volcanic Margin, Journal of Geophysical Research-Solid Earth 99, 9279-9296.

Raum, T., Mjelde, R., Berge, A.M., Paulsen, J.T., Digranes, P., Shimamura, H., Shiobara, H., Kodaira, S., Larsen, V.B., Fredsted, R., Harrison, D.J. and Johnson, M. (2005). Sub-basalt structures east of the Faroe Islands revealed from wide-angle seismic and gravity data, Petroleum Geoscience 11, 291-308.

Renard, F., Candela, T., Bouchaud, E. (2013) Constant dimensionality of fault roughness from the scale of micro-fractures to the scale of continents , Geophysical Research Letters 40, p. 83-87

Roberts, A. W., White, R. S., Lunnon, Z. C., Christie, P. A. F., Spitzer, R. and iSimm Team (2005), Imaging magmatic rocks on the Faroes margin. In: Petroleum geology: North-west Europe and global perspectives - Proceedings of the 6th Petroleum Geology Conference. Geological Society, London, Petroleum Geology Conference series 5, 755-766.

Rohrman, M. (2007). Prospectivity of volcanic basins: Trap delineation and acreage de-risking, AAPG Bulletin 91, 915-939.

Saunders, A.D. (2005). Large igneous provinces: origin and environmental consequences, Elements 1, 259-263.

Saupe, D., Algorithms for random fractals, in Peitgen, H., and Saupe, D., eds., The science of fractal images (Springer-Verlag, New York 1988).

Self, S., Keszthelyi, L., and Thordarson, T. (1998), The importance of pahoehoe, Annual Review of Earth and Planetary Sciences 26, 81-110.

Self, S., Widdowson, M., Thordarson, T., and Jay, A.E. (2006), Volatile fluxes during flood basalt eruptions and potential effects on the global environment: A Deccan perspective, Earth and Planetary Science Letters 248, 518-532.

Thomson, K. (2005), Volcanic features of the North Rockall Trough: application of visualisation techniques on 3D seismic reflection data, Bulletin of Volcanology 67, 116-128.

Thordarson, T., and Self, S. (1993), The Laki (Skaftar-Fires) and Grimsvotn eruptions in 1783-1785, Bulletin of Volcanology 55, 233-263.

Turcotte, D.L. (1989), Fractals in Geology and Geophysics, Pure and Applied Geophysics 131, 171-196.

Walia, R.K., and Bull, J.M. (1997), Modelling rough interfaces on seismic reflection profiles - The application of fractal concepts, Geophysical Research Letters 24, 2067-2070.

Welch, P. (1967), The use of fast Fourier transform for the estimation of power spectra: a method based on time averaging over short, modified periodograms, IEEE Transactions on Audio and Electroacoustics 15, 70-73.

Wessel, P., and Smith, W.H.F. (2009), The Generic Mapping Tools (GMT) version 4.5.0 Technical Reference & Cookbook, SOEST/NOAA, http://gmt.soest.hawaii.edu/.

White, J.C., Development and application of the phase-screen seismic modelling code (PhD thesis, Durham University 2009).

White, J. C. & Hobbs, R. W. (2007), Extension of forward modelling phase-screen code in isotropic and anisotropic media up to critical angle, Geophysics 72, SM107-SM114.

White, J.D.L., Bryan, S.E., Ross, P.-S., Self S., and Thordarson, T. (2009). Physical volcanology of continental large igneous provinces: update and review, in, Thordarson, T., Self, S., Larsen, G., Rowland, S.K., Hoskuldsson, A. (eds.), Studies in Volcanology: The Legacy of George Walker. Special Publications of IAVCEI 2, 291–321.

Figures
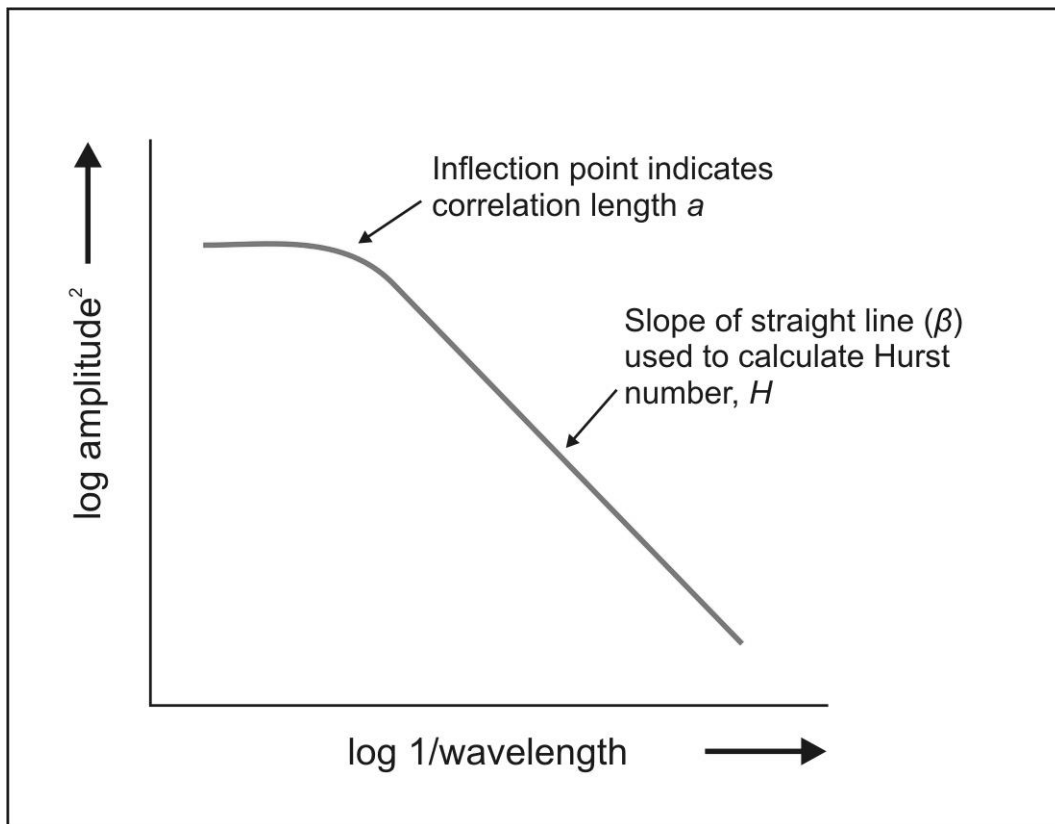
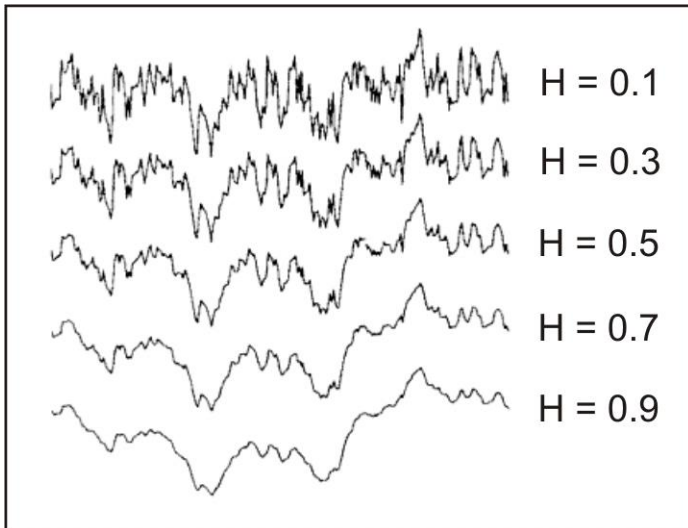**Figure 1**: Determining Hurst number and correlation length from a power spectrum.

Figure 2: Effect of the Hurst number on surface roughness, while the standard deviation remains constant. From Saupe (1988).
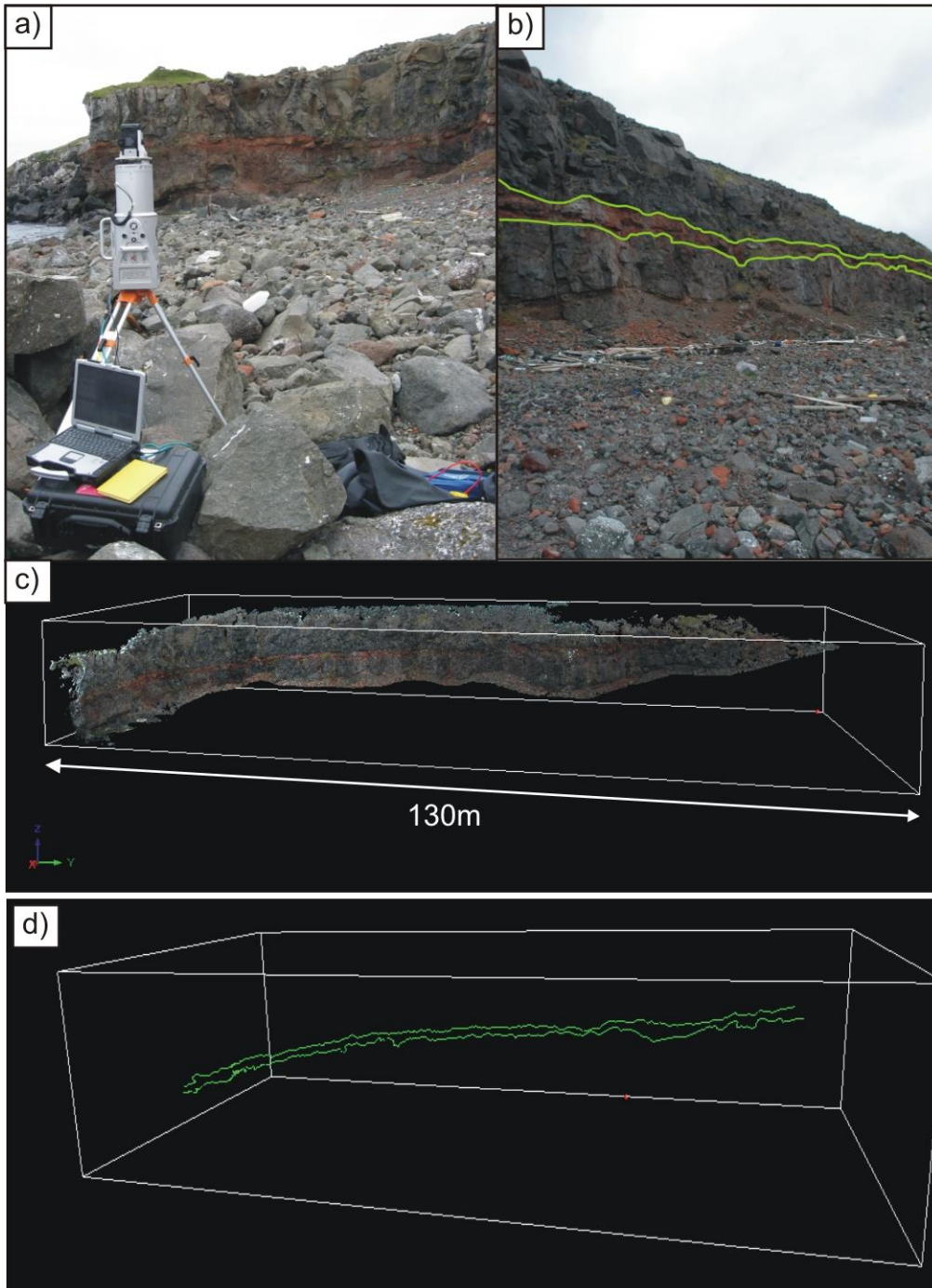
Figure 3: Laser scan data from coastal quarry at Glyvursnes. Outcrop height is approximately 10m. a) Acquiring the laser scan data. b) The quarry wall with photo-interpretation of the lava flow top and base. c) The completed scan data. d) Lines interpreted from the scan data.
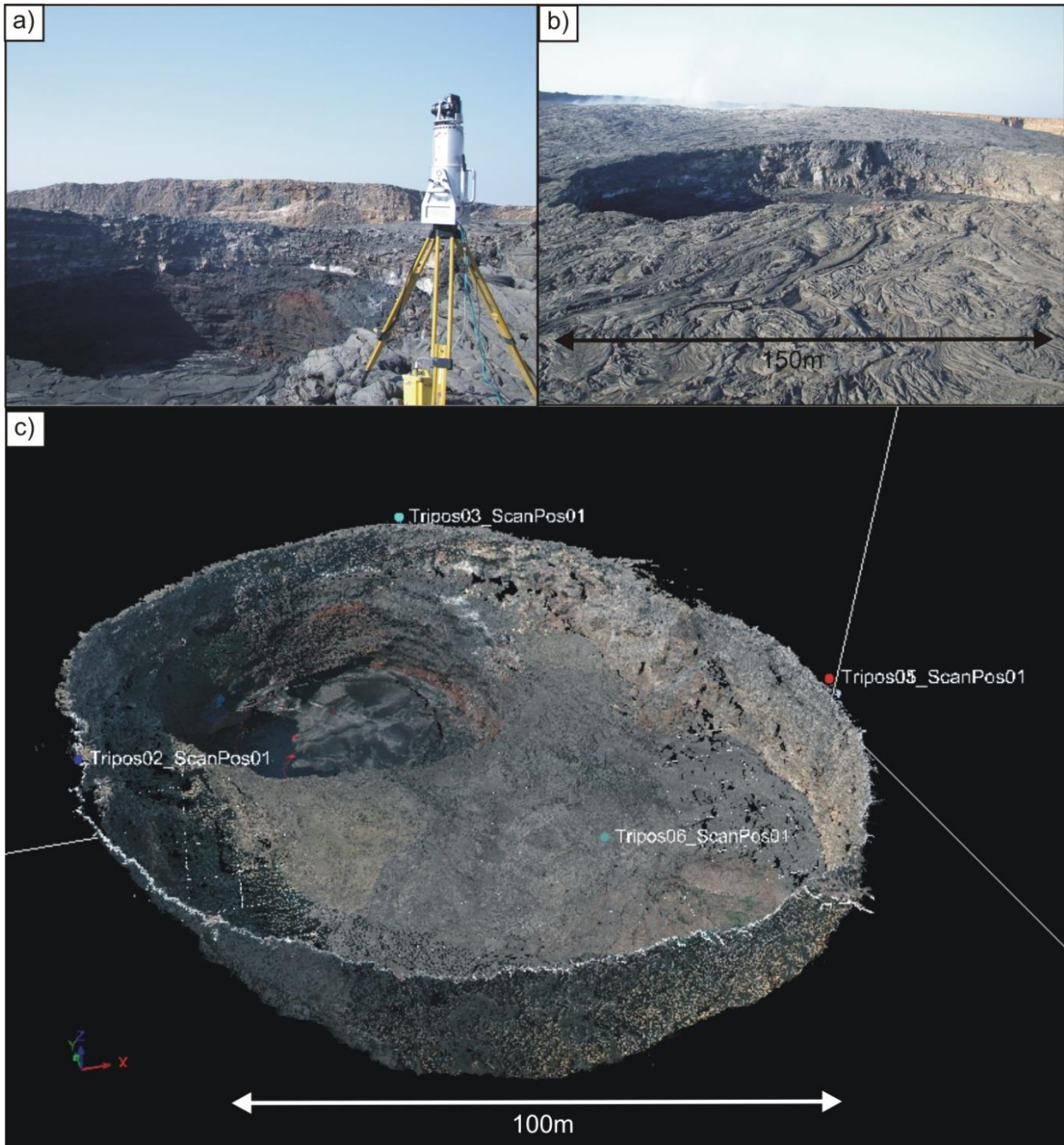
Figure 4: Laser scan data from Erta Ale, Ethiopia. Photographs courtesy of Dougal Jerram. a) Collecting

the scan data. b) Overview of the crater and surroundings. c) Complete scan data and scan positions.
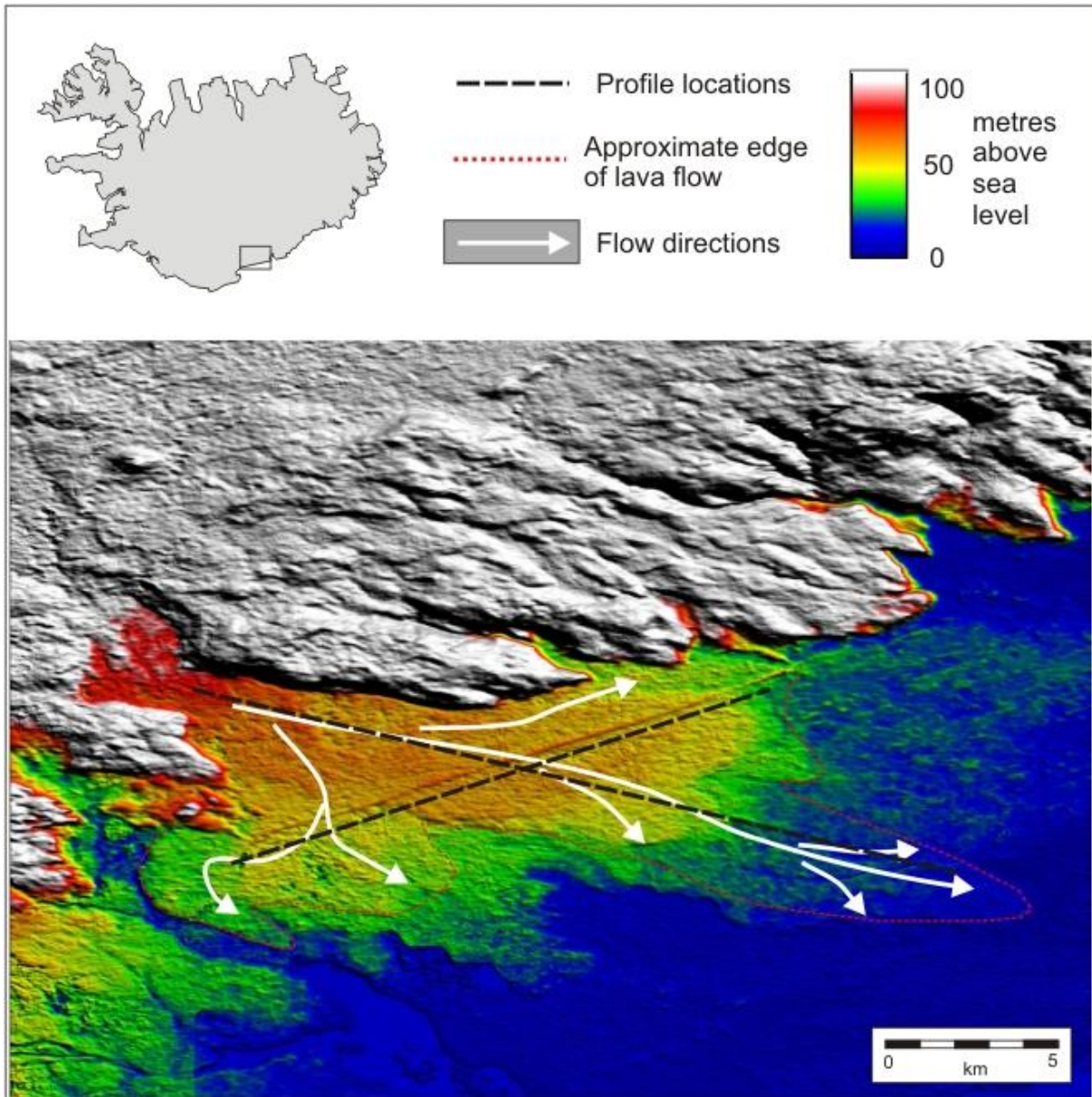
Figure 5: Eldhraun branch of the Laki lava flow: location map and satellite DEM from ASTER Global Digital Elevation Model (http://www.gdem.aster.ersdac.or.jp/). Data at 30m resolution. Original data of ASTER GDEM is the property of the Ministry of Economy, Trade and Industry (Japan) and NASA. Flow directions and Laki extent from Guilbaud et al. (2005).

Figure 6: Laki surface roughness. a) Eldhraun branch near Kirkjubaejarklaustur. b) Looking south across

the Eldhraun from Fjaðrárgljúfur.
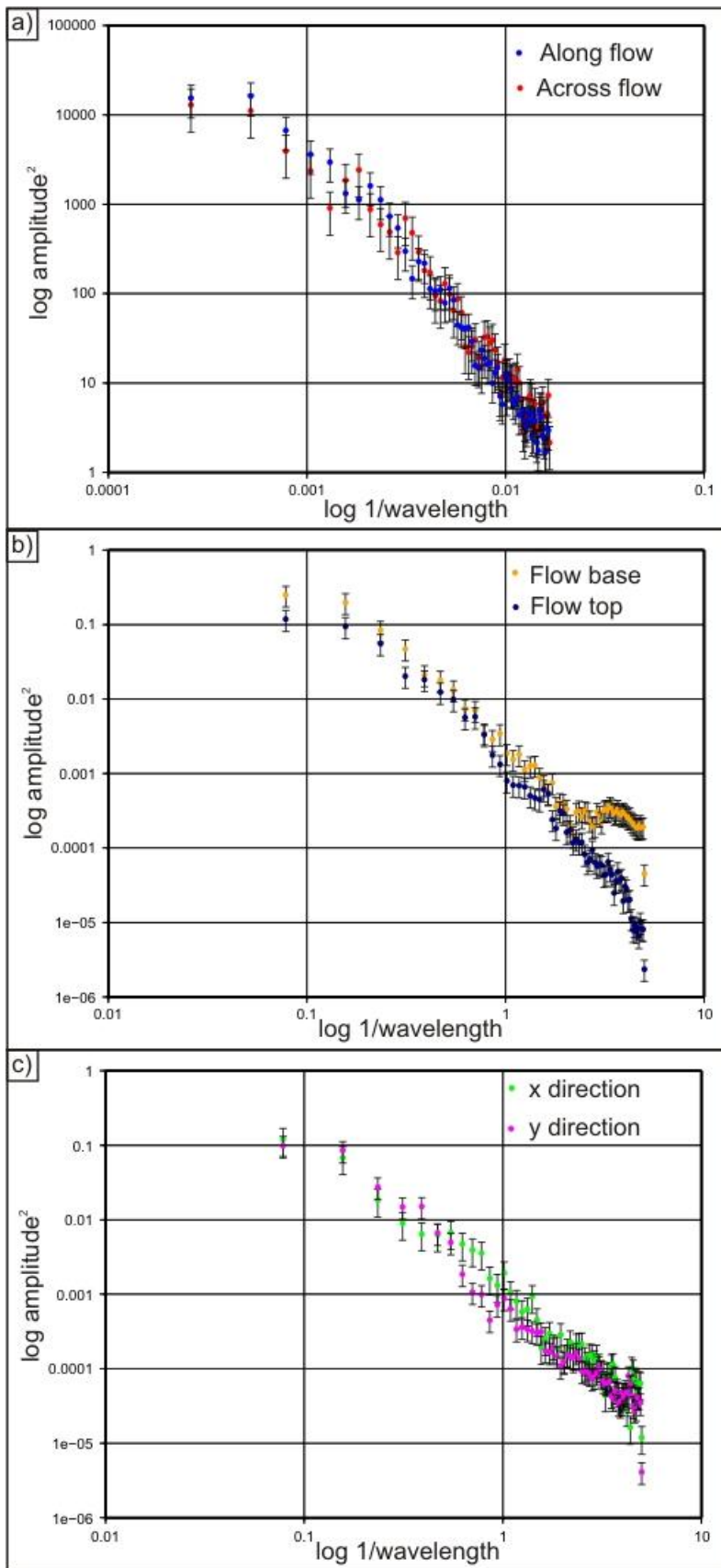
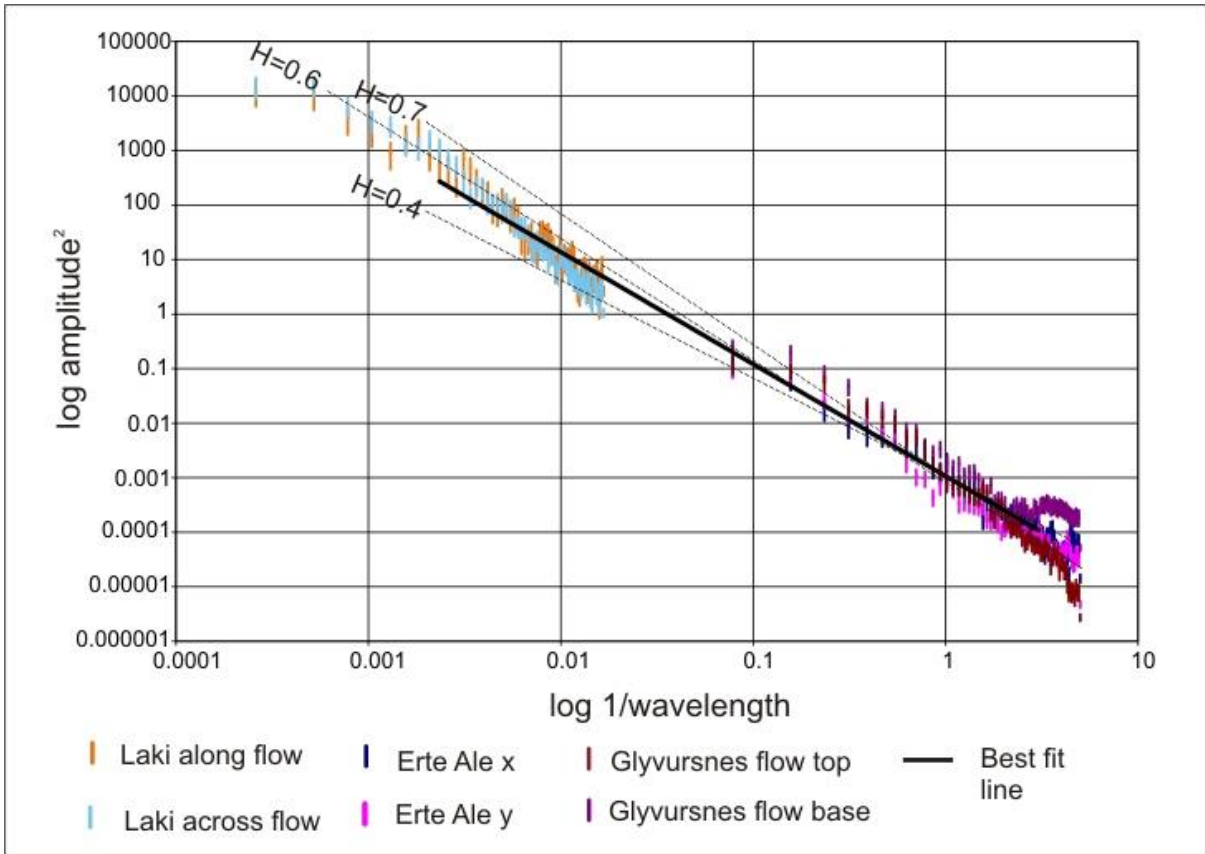**Figure 7:** Power spectra of data from a) Laki, b) Glyvursnes and c) Erte Ale.

Figure 8: All power spectra plotted together, only 1 standard deviation (s.d.) error bars shown. Dashed
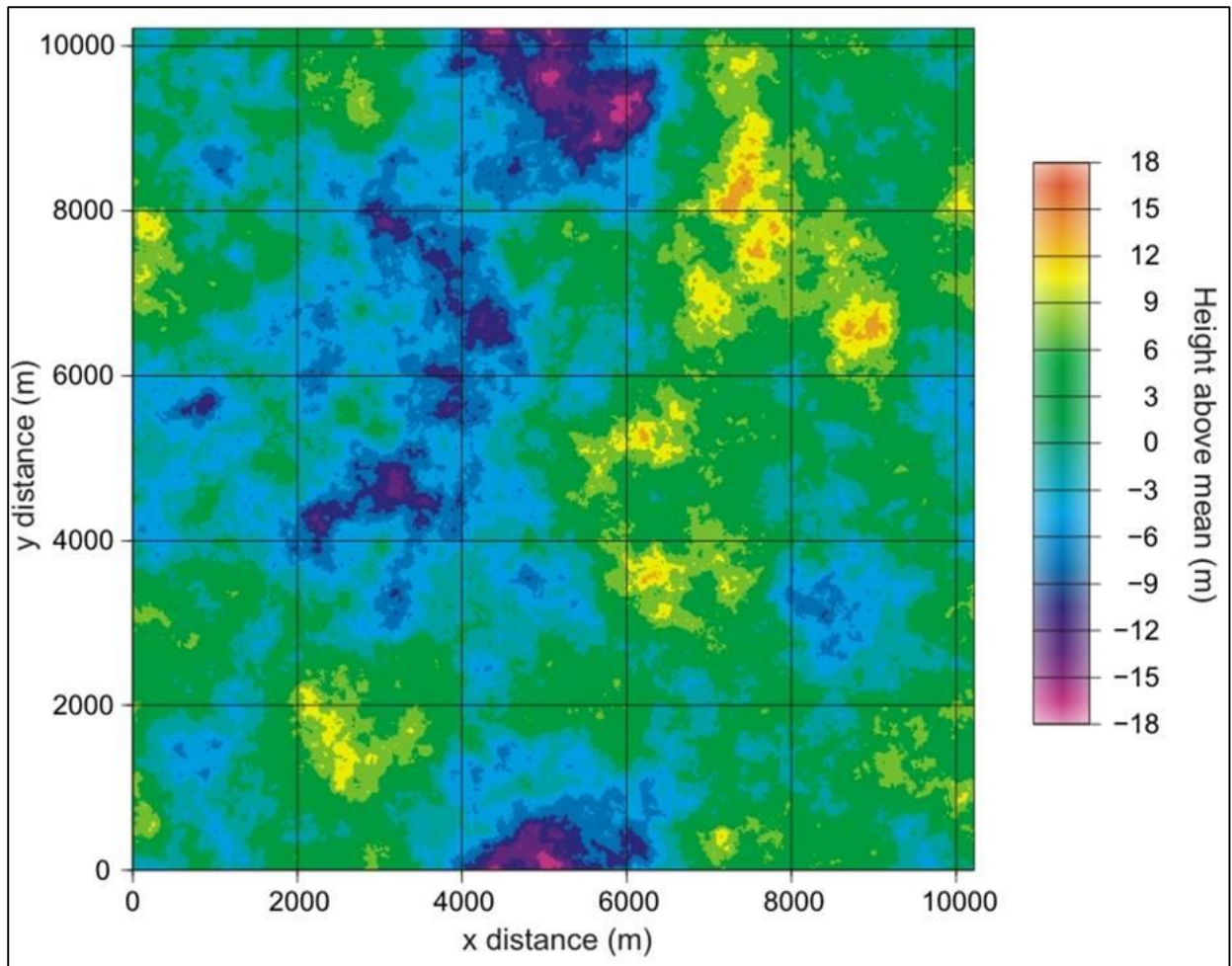
lines show other Hurst numbers for comparison.

Figure 9: Fractal model produced with the random volume building code of White (2009).
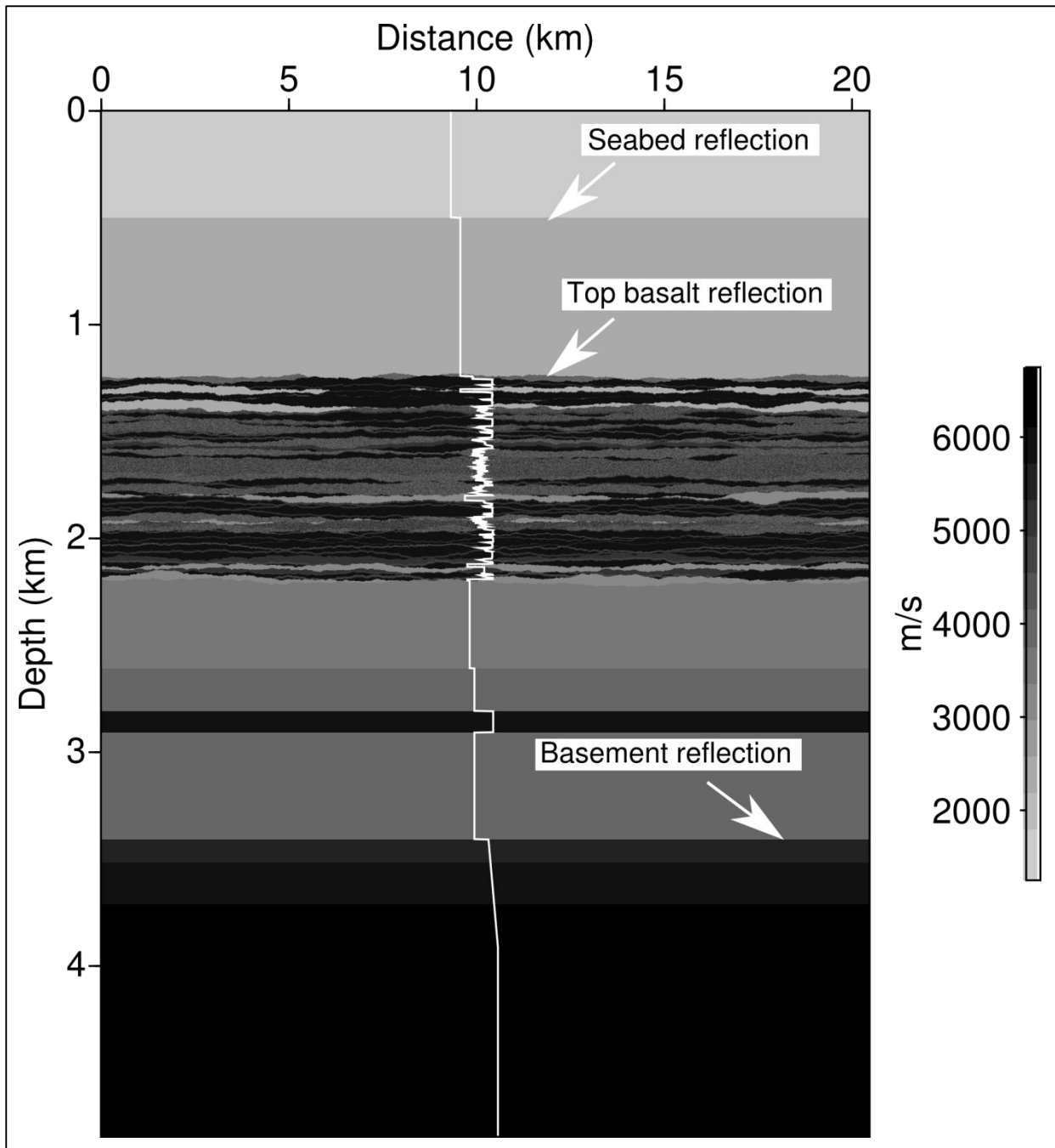
Figure 10: 2D section through a 3D probabilistic model for a sequence of flows that have built up a 2km thick basalt-dominated pile, which has then subsided and been buried by later sediments (similar to the Faroe-Shetland trough). The model is coloured by seismic P-wave velocity, but it could equally be coloured by density, S-wave velocity, or geological descriptors.
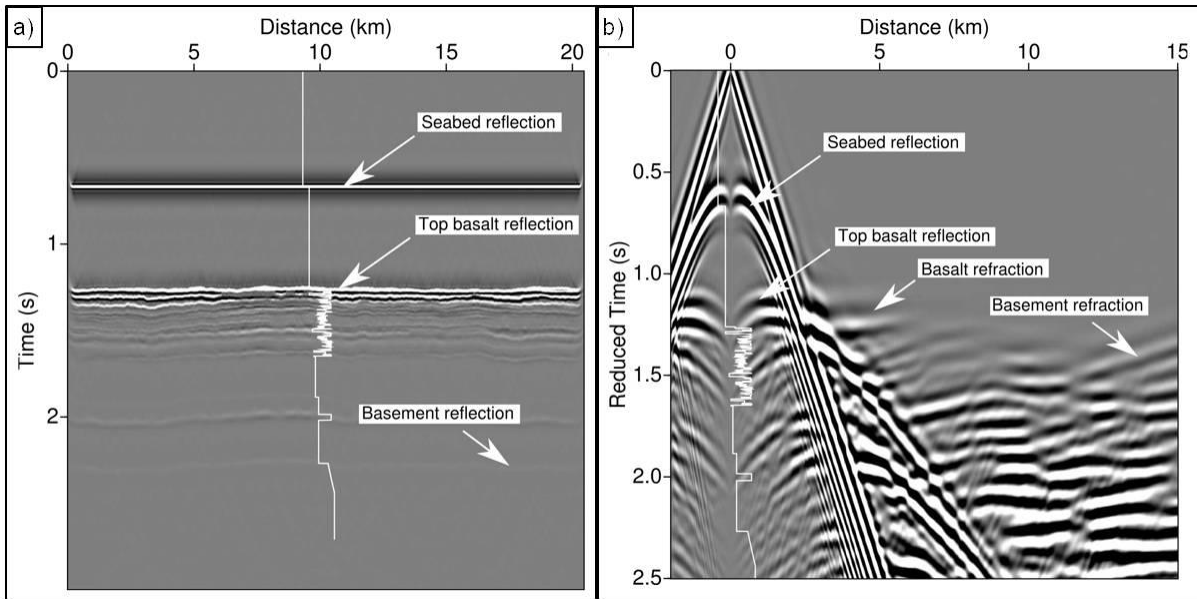
Figure 11: (a) Ideal primary only seismic reflection section from the model in figure 10 showing the rapid loss of back-scattered energy from the basalt sequence. In reality, the received image will be significantly degraded by the inclusion of the multiply scattered energy that will appear as noise on the section. (b) The corresponding long-offset refraction model. Note the termination of the basalt refraction event caused by multiple destructive interference of scattered energy which is dominated by scattering in the upper layers of the model.